EUROPEAN MECHANICAL SCIENCE
e-ISSN: 2587-1110

Research Article

The effect of the triangular rib usage in the plate fin heat sinks on the pressure drop, base plate temperature, and entropy generation

Muhammet Nasıf Kuru[1*]

[1]Vocational School of Technical Sciences at Mersin Tarsus Organized Industrial Zone, Machinery Program, Tarsus University, 33400, Tarsus, Mersin, Türkiye

Orcid: M. N. Kuru (0000-0002-5941-1221)

Abstract: Improving the thermal efficiency in plate fin heat sinks (PFHS) results in a reduction in the weight, volume, and cost of the heat sink. This also ensures the long life and reliable operation of the cooled equipment. In this study, the performances of triangular ribbed PFHSs, which are formed by placing a staggered array of triangular ribs between plate fins, were numerically investigated. Pressure drop, base plate temperature, and entropy generation are used for performance comparisons. Numerical heat transfer and flow analysis were performed in three-dimensional models with the help of the Ansys Fluent program, which uses the finite volume method with incompressible, turbulent flow and conjugate heat transfer assumptions. The design parameters were determined as inlet velocity between 3 m/s and 9 m/s, the number of plate fins 9, 12 and 15, plate fin heights 10 mm and 30 mm, and triangular rib heights 0.1 mm and 0.3 mm. As a result, the heat sink base plate temperature decreases with the increase of velocity, fin height, number of plate fins and triangular rib height, lower pressure drop values were obtained in the case of $H_{rib} = 0.1\ mm$ as compared to the unribbed case. If the design with the least entropy generation is desired as the optimum design, there is a 10.64% increase in the base plate temperature and a significant decrease in the pressure drop (220.88 Pa to 7.512 Pa). In this case, since the fin length is $H = 30\ mm$, the volume and weight of the heat sink also increase.

Keywords: heat sink, plate fin, triangular rib, entropy generation, base plate temperature, pressure drop, thermal resistance.

1. Introduction

Efficient heat removal in heat sinks is very important for compact design, effective energy use, safe operation, and long operating life of the cooled equipment. In heat sinks, the thermal efficiency can be increased in two ways as active and passive methods. The passive method is frequently used because it improves thermal efficiency without the need for additional energy. The thermal hydraulic efficiency of heat sinks depends on the heat transfer and pressure drop, and many different methods are used to compare the thermal hydraulic efficiency. The entropy generation minimization method proposed by Bejan [1] is one of the most popular methods for comparing the efficiency of heat sinks. Thus, heat transfer and pressure drop are evaluated together.

Plate finned heat sinks are frequently preferred in cooling applications due to their simple structure and easy production. Since PFHSs cause laminar flow, they do not provide the desired improvement in heat transfer and are insufficient in applications where low volume cooling is required [2]. Therefore, different geometries, design conditions, and dimensions have been studied by researchers to increase thermal hydraulic efficiency in PFHSs. Yu et al. [3] added pin fins between the plate fins in their PFHS and obtained approximately 30% less thermal resistance with the new type heat sink at the same velocity compared to the PFHS. In addition, Yuan et al. [4], Yamaç and Koca [5] improved heat transfer by using plate fin and pin fin together in heat sinks.

Ayli et al. [6] investigated the heat transfer characteristics numerically and experimentally by placing the plate fin structure perpendicular to the flow in the square section channel. Inci and Bayer [7] numerically investigated the effect of using plate fins, square and circular pin fins on heat transfer in heat sinks. Gupta et al. [8] investigated the heat transfer and flow characteristics by pitting the plate fin surfaces in PFHSs. The study was carried out for cases where the Reynolds number varies between 6800 and 15200. As a result, they found that the dimpled PFHSs have higher heat transfer, friction factor, and fin efficiency than the PFHSs. Shaeri and Yaghoubi [9] increased the thermal efficiency of PFHSs by drilling

* Corresponding author.
Email: mnasifkuru@tarsus.edu.tr

European Mechanical Science (2023), 7(2): 99-108
https://doi.org/10.26701/ems.1276575
Received: April 4, 2023 — Accepted: May 22, 2023

square holes in the direction of flow. The Reynolds number ranges from 100 to 350. The number of square holes varied from 1 to 8. As a result, they found that the heat transfer was improved with the use of square holes, the weight of the heat sink was reduced, and the 8-hole PFHS had 35% fin effectiveness for the Reynolds number of 350.

Ahmed and Ahmed [10] numerically investigated the heat transfer characteristics of microchannel heat sinks with triangular, trapezoidal, and rectangular grooves and determined the optimum thermal design parameters. As a result, they found that the trapezoidal groove provided 51.59% improvement in Nusselt number and 2.35% increase in friction factor. Ahmed [11] numerically investigated the optimization of the thermal design of ribbed plate fin heat sinks. It was determined that the thermal efficiency with the use of ribs was 1.55 times higher than that of the flat plate fin, and it was stated that this improvement decreased as the number of ribs increased. The use of rib at the same thermal efficiency resulted in a 69.65% reduction in pumping power. Khudhur et al. [12] investigated the heat transfer characteristics by experimental and numerical methods by applying the process of adding and removing protrusions in plate fin heat sinks. The Reynolds number ranges from 6300 to 35120. It was stated that the heat sinks with protrusion insertion and subtraction are more effective in dissipating heat than the flat plate finned heat sinks.

Li et al. [13] used delta fin vortex generators to improve heat transfer in a plate fin heat sink. The experimental and numerical work is modeled for the cross-flow state in the channel. The distance between the trailing edges of the vortex generators, the distance between each vortex generator and the heat sink, the angle of attack of the vortex generators, and the height and arrangement of the vortex generators are considered as design parameters. In order to optimize the thermal resistance and pressure difference, the angle of attack of the vortex generator is 30°. As a result, it has been determined that the improvement in heat transfer is greater and the increase in pressure drop is less with the use of a vortex generator at low Reynolds numbers. Huang and Tung [14] investigated the optimum design of the deformed wave heat sink numerically and experimentally. In optimization problems, the objective function is the minimization of the heat sink base plate temperature and constant volume is assumed as a constraint. As a result, the deformed wavy heat sinks with the optimization studies were compared with the flat plate fin heat sinks, and a reduction in the base plate temperature of the heat sink between 8.78% and 1.35% was obtained. Experimental studies were carried out to verify the numerical results obtained. Bouchenafa and Mohammed [15] numerically investigated the thermal hydraulic efficiency of wavy plate fin heat sinks. The wave numbers and the amplitude of the waves were determined as the operating parameters and the obtained results were compared with the plate fin heat sinks. The lowest thermal resistance was obtained at the highest values of wave number and amplitude (5 mm and 4 mm, respectively).

In this study, the performances of the triangular ribbed PFHSs created by placing the triangular ribs with a staggered arrangement between the PFHSs were numerically investigated. Pressure drop, base plate temperature, and entropy generation are used for performance comparisons. Numerical heat transfer and flow analysis were performed with the help of the Ansys Fluent program using the finite volume method. The studied design parameters and ranges were inlet velocity (from 3 m/s to 9 m/s), number of plate fins (9, 12 and 15), plate fin height (10 mm and 30 mm), and triangular rib height (0.1 mm and 0.3 mm).

2. Material and Method

Schematic diagrams of PFHS and triangular ribbed PFHS are shown in Figure 1. For the triangular ribbed PFHS, 4 equilateral triangle type rib with a staggered arrangement is placed on plate fins in the flow direction.

The solution domain and geometric dimensions for PFHS and triangular ribbed PFHS are shown in Figure 2. In order to save computation time, the solution domain is defined where the number of plate fin is $N_{fin} = 1$. The geometric and operating parameters of the heat sinks are listed in Table 1. Air is used as the working fluid and it

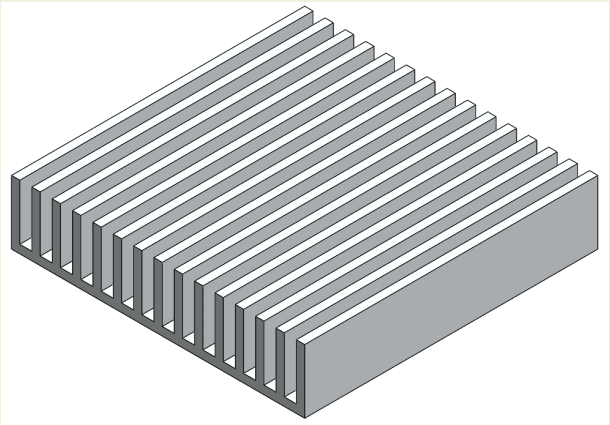

(a)

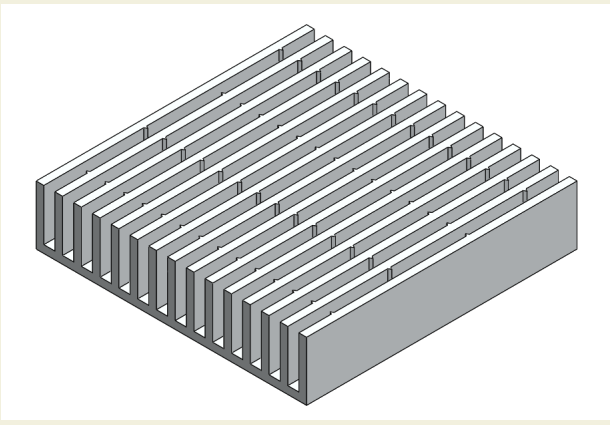

(b)

Figure 1. Schematic diagram of (a) PFHS (b) triangular ribbed PFHS

approaches the heat sink at an inlet velocity of V_{in}. The material of the heat sinks is aluminum. The solution domain consists of two zones (solid and fluid), fluid zone consists of three sections, namely inlet, test and exit. Temperature and pressure drop measurements are done at the entrance and exit of the test zone. The test zone is 100 mm long and centered on the heat sink. The Cartesian coordinate system was used to describe heat and fluid flow. The thermo-physical properties of air and aluminum were assumed to be constant and were taken from Incropera [16].

2.1. Conservation Equations:

Continuity, momentum, energy and turbulence equations are the governing equations in numerical heat and flow calculations. Heat and flow studies were performed using three-dimensional models, assuming incompressible, turbulent flow and conjugate heat transfer. Continuity, momentum and energy equations in Cartesian coordinates are given below ([17], [18])

Continuity Equation:

$$\frac{\partial}{\partial x_i}(u_i) = 0 \tag{1}$$

Momentum Equation:

$$\rho_{air}\, u_j \frac{\partial u_i}{\partial x_j} = -\frac{\partial p}{\partial x_i} + \frac{\partial}{\partial x_j}\left[(\mu + \mu_t)\frac{\partial u_i}{\partial x_j}\right] \tag{2}$$

Energy Equation:

$$\rho_{air}\, u_j \frac{\partial T}{\partial x_j} = \frac{\partial}{\partial x_j}\left[\left(\frac{\mu}{Pr} + \frac{\mu_t}{Pr_t}\right)\frac{\partial T}{\partial x_j}\right] \tag{3}$$

Renormalization Group (RNG) k-ε turbulence model with enhanced wall treatment is used in this study, detailed formulations are given in [19].

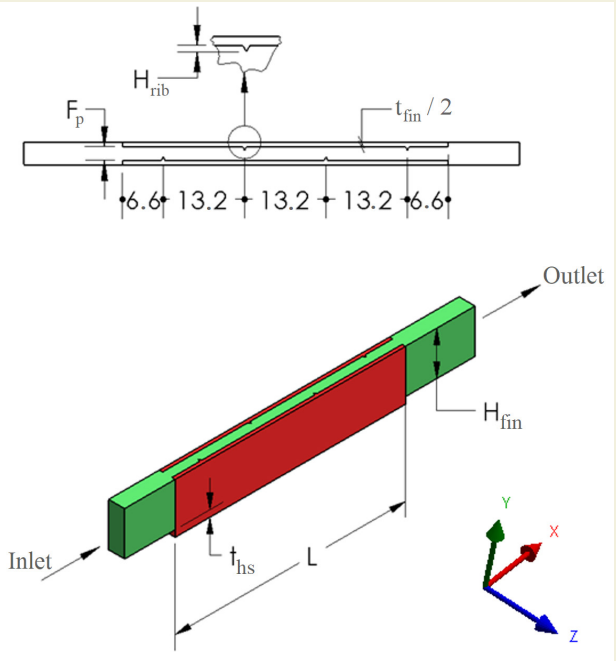

Figure 2. Solution domain and dimensions of (a) PFHS (b) triangular ribbed PFHS (all dimensions are in millimeters)

2.2. Data Analysis

The thermal resistance R_{th} of the heat sink is calculated by the formula:

$$R_{th} = \frac{\Delta T}{\dot{Q}} \tag{4}$$

$\dot{Q}$ is the heat transfer. ΔT is the temperature difference, it is defined as the difference between the heat sink base plate temperature and the inlet temperature:

$$\Delta T = (T_{base} - T_{in}) \tag{5}$$

Reynolds number is defined as:

$$Re_{d_h} = \frac{V_{in}\, d_h}{\upsilon} \tag{6}$$

υ is the kinematic viscosity of air. d_h is the hydraulic diameter of the wind tunnel and

$$d_h = \frac{2\, CH\, CB}{CH + CB} \tag{7}$$

Inlet velocity is

$$V_{in} = \frac{\dot{V}_{flow}}{A_{channel}}\, V_{in} \tag{8}$$

$\dot{V}_{flow}$ is the volumetric flow rate, $A_{channel}$ is the cross-sectional area of the wind tunnel, A_{front} is the frontal area of the fins

$$A_{channel} = CH\, CB \tag{9}$$

$$A_{front} = N\, H\, t_{fin} \tag{10}$$

ΔP is the difference between the pressure values measured at the inlet and outlet of the heat sink. The entropy generation rate in heat sinks is calculated using the Bejan's [1] formula as follows:

Table 1. Geometric and operating parameters of the heat sink in this study

Parameter	Symbol	Unit	Range/Value
Fin length	L	mm	52.8
Fin height	H_{fin}	mm	10 and 30
Fin width	B	mm	52.8
Number of fins	N	-	9, 12 and 15
Pitch between plate fins	F_p	mm	4.913, 3.164 and 2.164
Fin thickness	t_{fin}	mm	1.5
Base plate thickness of heat sink	t_{hs}	mm	1.5
Rib height	H_{rib}	mm	0.1 and 0.3
Height of channel	CH	mm	10 and 30
Width of channel	CB	mm	52.8
Heat load	$\dot{Q}$	W	10
Inlet velocity	V_{in}	m/s	3, 5, 7, 9
Inlet temperature	T_{in}	°C	21.3

$$\dot{S}_{gen} = \frac{\dot{Q}^2 R_{th}}{T_{in}^2} + \frac{\Delta P \dot{V}_{flow}}{T_{in}} \quad (11)$$

2.3. Numerical Method and Boundary Conditions:

Ansys Workbench program is used to create the three-dimensional geometric models and mesh of heat sinks and to perform their numerical analysis. Geometric models are created with Ansys Design Modeler, geometric models are meshed with Ansys Mesher and numerical analysis are done with Ansys Fluent which uses the finite volume method. The second-order upwind scheme is used in the numerical analysis of the conservation and turbulence equations. The COUPLED algorithm was chosen for velocity and pressure coupling because of its fast convergence. The convergence criterion is set to be less than 10^{-5} for the continuity, momentum, and turbulence equations and less than 10^{-9} for the energy equation.

For the mesh structure, hexahedral elements were used in the entrance, exit and wall sections, and tetrahedral elements were used in the test section. In addition, the mesh structure near the wall surface has been tightened so that the y+ value is kept between 1 and 5. The mesh of the triangular ribbed PFHS is shown in Figure 3.

The boundary surfaces of PFHS and triangular ribbed PFHS are marked in Figure 4, and the boundary conditions are summarized in Table 2 with mathematical expressions.

2.4. Mesh Independency

For the accuracy of the numerical results obtained, the mesh of the numerical models should be checked. In addition, a sufficient number of elements should be selected in terms of computation time and cost. For this reason, the mesh independence study for 4 different element numbers on the numerical model of PFHS used in the validation studies was performed for $Re_{d_h} = 14006$. The variation of thermal resistance and pressure drop with the number of elements is shown in Figure 5. For the mesh with the last two element numbers, the deviations are around 0.95% for the thermal resistance and 0.98% for the pressure drop. In order to save computation time, the third mesh with the number of elements 2.09E+6 is used in this study.

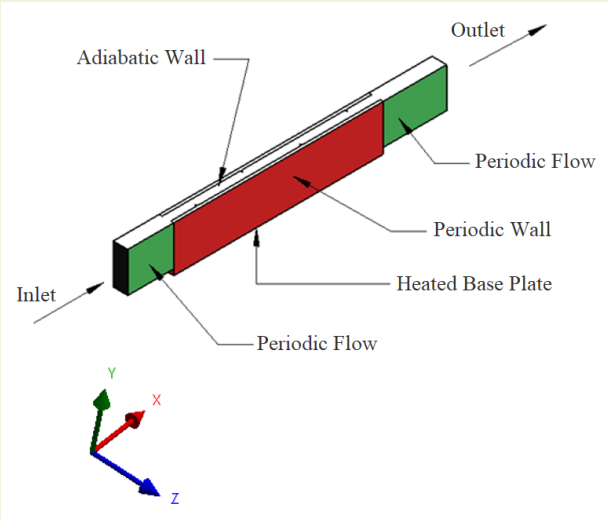

Figure 4. Boundary conditions for triangular ribbed PFHS

2.5. Validation Study

Experimental data obtained in terms of thermal resistance and pressure drop in Jonsson and Moshfegh's [20] PFHSs work were used to validate the numerical studies. Comparison results are shown in Figure 6 for thermal resistance (R_{th}) vs. Reynolds number (Re_{d_h}), in Figure 7 for pressure drop (ΔP) vs. Reynolds number (Re_{d_h}). As can be seen from the results, the current numerical study results agree with the experimental data, there is a deviation between 6.66% and 12.46% in the thermal resistance and between 0.39% and 12.4% in the pressure drop, according to the experimental data.

3. Results and Discussions

In this study, performance comparisons are done for PFHS and triangular ribbed PFHS where the inlet velocity varies between 3 m/s and 9 m/s, the number of plate fins is 9, 12 and 15 (the pitch between plate fins corresponds to 4.913 mm / 3.164 mm / 2.164 mm), the height of the fin is 10 mm and 30 mm, the height of the rib is 0.1 mm and 0.3 mm. The pressure drop, base plate temperature and entropy generation values between the test zone inlet and outlet of the heat sink were selected for performance comparisons.

3.1. The effect of the studied parameters on the pressure drop (ΔP):

The variation of pressure drop (ΔP) with inlet velocity (V_{in}) is shown in Figure 8 for the studied parameters. For PFHS and triangular ribbed PFHS, the pressure drop increases with the increasing inlet velocity. The pressure drop decreases with the increasing fin pitch between fins (F_p) (or decreasing the number of fins). Rib height is important, as ribs disturb thermal boundary layer development, resulting in improved heat transfer. At the same values of F_p, regardless of $H = 10\ mm$ or $H = 30\ mm$, if the rib height is $H_{rib} = 0.1\ mm$, the pressure drop is lower as compared to PFHS. However, the highest pressure drop value is reached at the same F_p when $H_{rib} = 0.3\ mm$. The maximum pressure drop value was obtained when $H = 10\ mm, F_p = 2.164\ mm, N = 15, H_{rib} = 0.3\ mm$. It

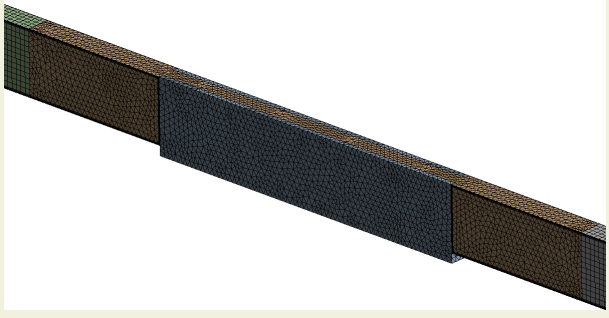

Figure 3. Mesh of the triangular ribbed PFHS (shown around the test section)

Table 2. Boundary Conditions

Body / Surface	Boundary Condition Type	Explanation	Mathematical Expression
Inlet	velocity-inlet	The velocity and temperature distributions are uniform and constant.	$u = V_{in}, v = 0, w = 0,$ $T_{in} = 21.3\ ^{\circ}C$
Outlet	pressure-outlet	The outlet pressure is equal to the atmospheric pressure, the velocity and temperature gradients in the x direction are equal to zero.	$P = P_{atm}$ $\frac{\partial u}{\partial x} = \frac{\partial v}{\partial x} = \frac{\partial w}{\partial x} = 0, \frac{\partial T}{\partial x} = 0$
Periodic flow	periodic	It is assumed that fluid velocities and temperatures at the z = 0 and z = F_p surfaces are equal.	$u_{(z=F_p)} = u_{(z=0)}$ $v_{(z=F_p)} = v_{(z=0)}$ $w_{(z=F_p)} = w_{(z=0)}$ $T_{(z=F_p)} = T_{(z=0)}$
Heated Base Plate	wall	Non-slip boundary condition and constant heat flux are applied. Heat flux is obtained by dividing $\dot{Q} = 10\ W$ by the base surface area of the heat sink (52.8 mm x 52.8 mm).	$u = 0, v = 0, w = 0$ $q" = 3587\ \frac{W}{m^2}$
Adiabatic wall	wall	Non-slip boundary condition is applied, it is assumed that the wind tunnel is well insulated and there is no heat loss to the outside.	$u = 0, v = 0, w = 0$ $\frac{\partial T}{\partial x} = \frac{\partial T}{\partial y} = \frac{\partial T}{\partial z} = 0$
Periodic wall	periodic	It is assumed that wall temperatures at the $z = 0$ and $z = F_p$ surfaces are equal.	$u = 0, v = 0, w = 0$ $T_{wall,(z=F_p)} = T_{wall,(z=0)}$
PFHS	coupled	Conjugate heat transfer is applied between the heat sink and the air.	$k_{air} \frac{\partial T_{air}}{\partial n} = k_{hs} \frac{\partial T_{hs}}{\partial n}$

Table 3. Geometric and operating parameters of the heat sink in the validation study

Parameter	Symbol	Unit	Range/Value
Fin length	L	mm	52.8
Fin height	H_{fin}	mm	10
Fin width	B	mm	52.8
Number of fins	N	-	9
Pitch between plate fins	F_p	mm	5
Fin thickness	t_{fin}	mm	1.5
Height of channel	CH	mm	10
Width of channel	CB	mm	63
Frontal area	A_{front}	cm^2	1.4
Heat load	$\dot{Q}$	W	10
Reynolds number	Re_{d_h}	-	2699, 5544, 7518, 11465, 14006
Inlet velocity	V_{in}	m/s	3.76, 5.10, 7.78, 9.51
Inlet temperature	T_{in}	°C	21.3

is seen that the pressure drop decreases with the increase in the fin height.

3.2. The effect of the studied parameters on the base plate temperature of the heat sink (T_{base}):

In Figure 9, heat sink base plate temperature (T_{base}) vs. inlet velocity (V_{in}) variation is given for the studied parameters. As the inlet velocity increases, the heat sink base plate temperature decreases. As the fin height (H) increases from 10 mm to 30 mm, T_{base} generally decreases, and T_{base} decreases by 34% at $F_p = 4.913\ mm, N = 9$ for PFHS. The highest base plate temperatures were obtained for the same F_p and V_{in} values in the PFHSs. T_{base} decreases as the fin height and the number of

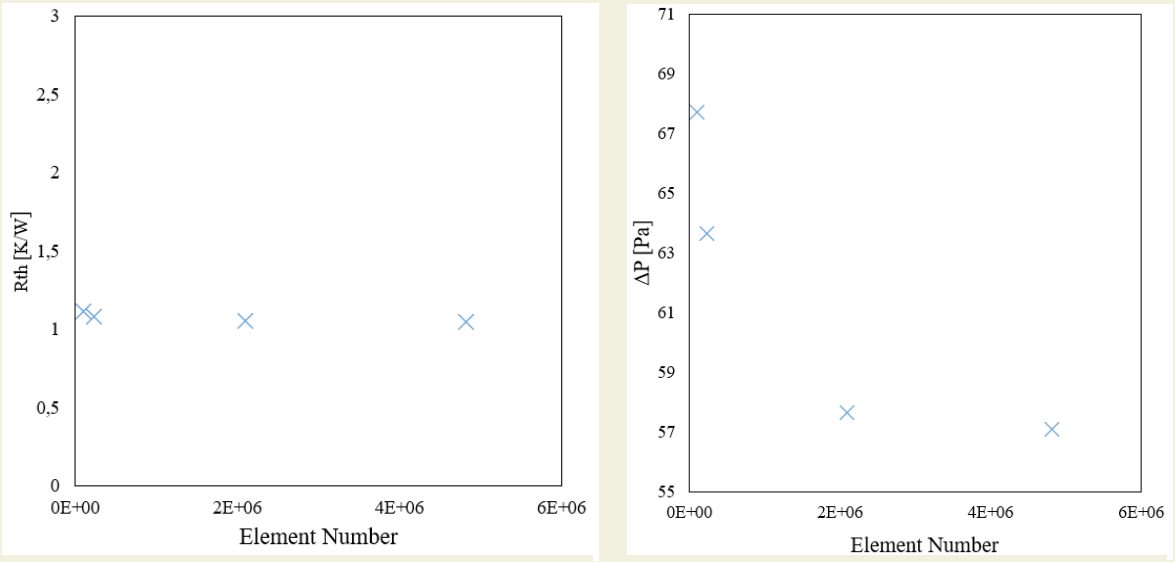

(a) (b)

Figure 5. Element number vs. (a) thermal resistance, R_{th} (b) pressure drop, ΔP

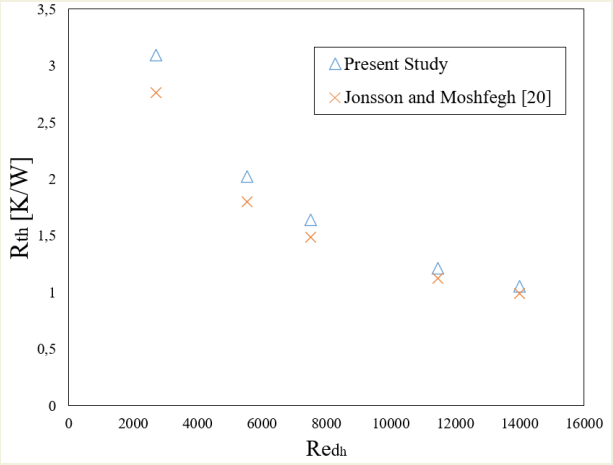

Figure 6. A validation study, thermal resistance (R_{th}) vs. Reynolds number (Re_{d_h})

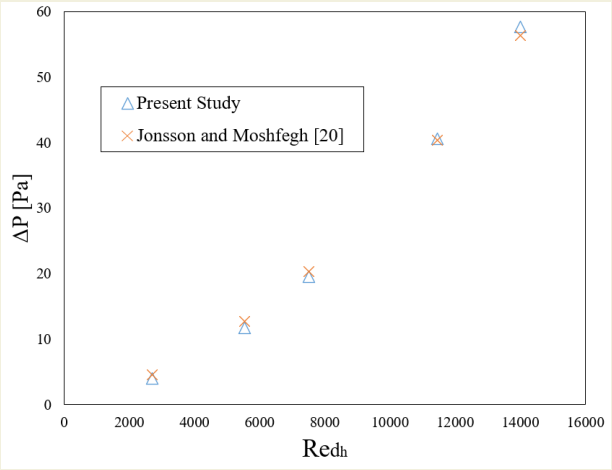

Figure 7. A validation study, pressure drop (ΔP) vs. Reynolds number (Re_{d_h})

fins increase. For $F_p = 2.164\ mm$ and $N = 15$, increasing the rib height decreases T_{base} slightly. In addition, increasing the fin height provides a decrease between 5% and 15% in T_{base} for the studied V_{in} values where $F_p = 2.164\ mm$ ve $N = 15$.

3.3. The effect of the studied parameters on the entropy generation ($\dot{S}_{gen}$) :

The variation of entropy generation ($\dot{S}_{gen}$) with inlet velocity (V_{in}) is illustrated for the studied parameters in Figure 10. In order to obtain meaningful graphics on the figures, the cases are discussed at the same values of F_p and N. In general, $\dot{S}_{gen}$ increases as the velocity increases. The lowest base plate temperature is obtained as $T_{base} = 22.053\ °C$ when $H = 30\ mm, F_p = 2.164\ mm, N = 15, H_{rib} = 0.3\ mm, V_{in} = 9\ m/s$. In this case, the pressure drop value is $\Delta P = 220.88$ Pa and the entropy generation value reached the highest value ($\dot{S}_{gen} = 0{,}01078\ W/K$). The lowest entropy generation is obtained as $\dot{S}_{gen} = 0{,}000479\ W/K$ at $H = 30\ mm, F_p = 4.913\ mm, N = 9, H_{rib} = 0.1\ mm, V_{in} = 3\ m/s$. In this case, the base plate temperature is $T_{base} = 24.401\ °C$ and the pressure drop is $\Delta P = 7.512\ Pa$. This value leads to 10.64% increase in the base plate temperature compared to the design at the lowest base plate temperature. However, the pressure drop values decreases significantly from 220.88 Pa to 7.512 Pa, which significantly reduces the pressure drop effects in entropy generation. If a slight increase in base plate temperature is acceptable for the design with the least entropy generation, there will be a significant reduction in pressure drop and hence fan power.

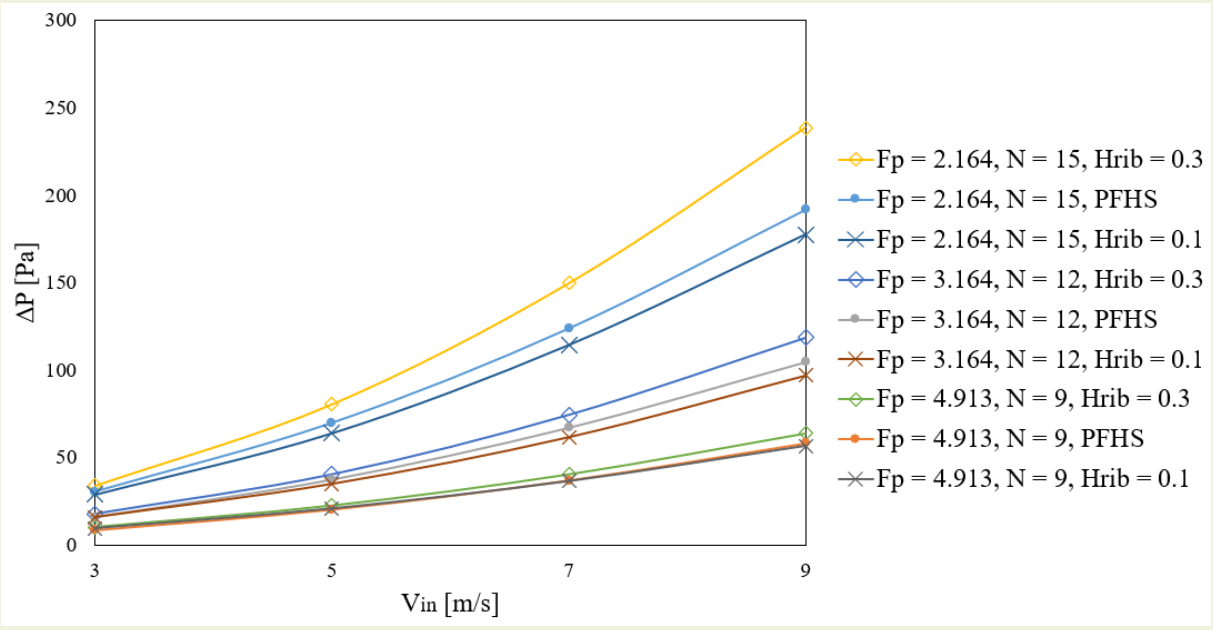

(a)

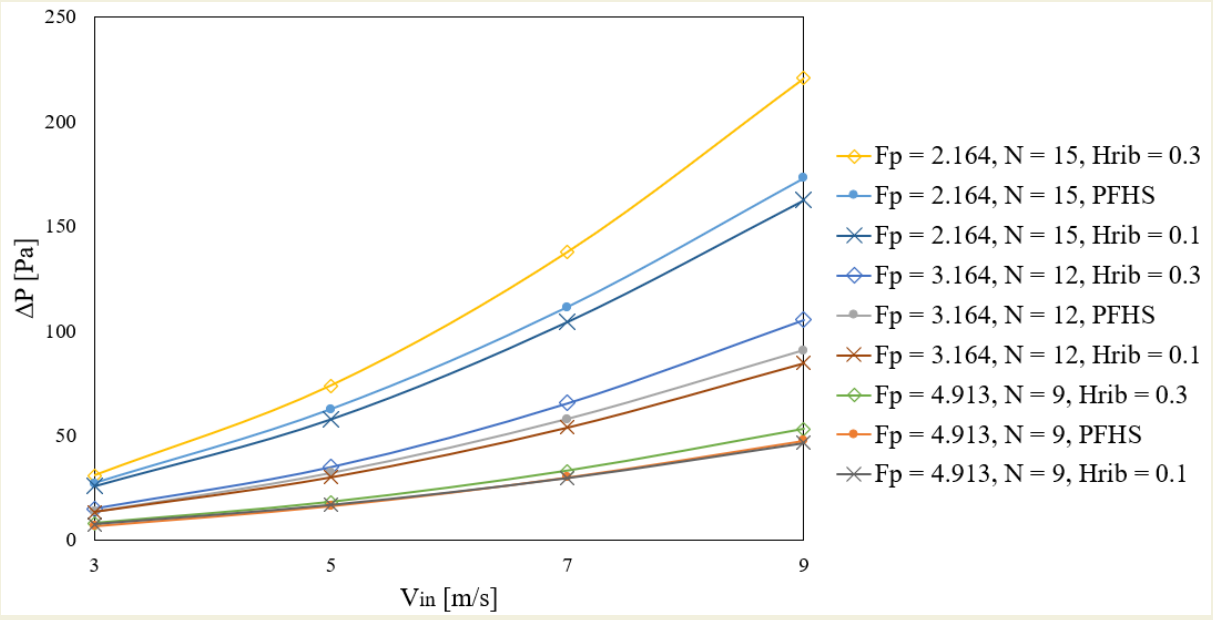

(b)

Figure 8. Pressure drop (ΔP) vs. inlet velocity (V_{in}) (a) $H = 10\ mm$ (b) $H = 30\ mm$

4. Conclusions

Performance comparisons for various parameters (inlet velocity, number of plate fins/pitch between fins, plate fin height, rib height) in PFHSs and triangular ribbed PFHSs were made in terms of pressure drop, base plate temperature and entropy generation values. The following results were obtained:

- It has been determined that the pressure drop decreases with the increase in the pitch between plate fins (F_p) (or the decrease in the number of fins) and the pressure drop increases with the increase in the inlet velocity.
- The pressure drop value decreases when $H_{rib} = 0.1\ mm$ as compared to PFHS. The pressure drop value is maximum for $H = 10\ mm, F_p = 2.164\ mm, N = 15, H_{rib} = 0.3\ mm$.
- As the inlet velocity increases, the heat sink base plate temperature decreases as expected. The highest heat sink base plate temperature is obtained in the PFHSs. The heat sink base plate temperature has the lowest value as $T_{base} = 22{,}053\ °C$ where $H = 30\ mm, F_p = 2.164\ mm, N = 15, H_{rib} = 0.3\ mm, V_{in} = 9\ m/s$. In this case, pressure drop and entropy generation values reach the maximum values as $\Delta P = 220.88$ Pa and $\dot{S}_{gen} = 0.01078\ W/K$, respectively.

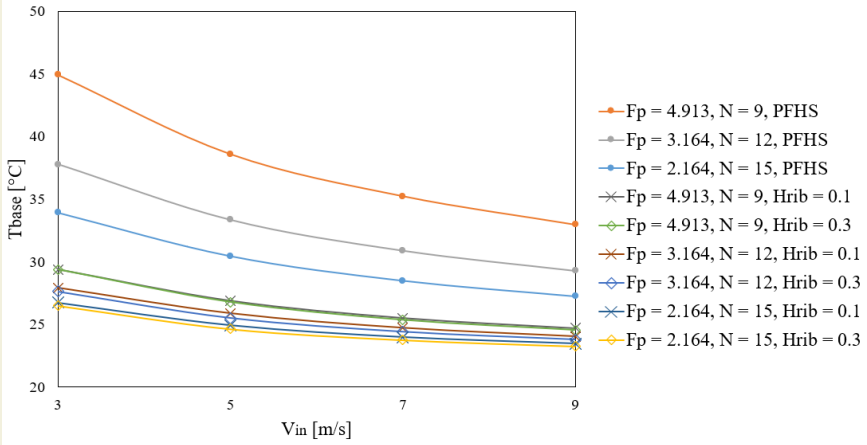

(a)

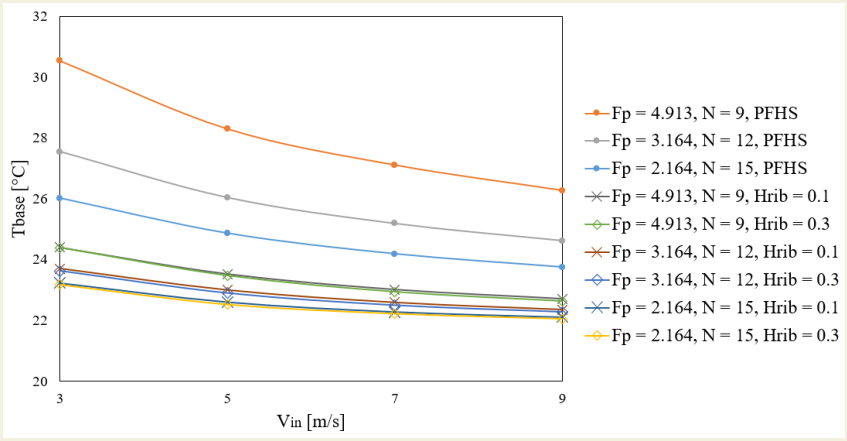

(b)

Figure 9. Heat sink base plate temperature (T_{base}) vs. inlet velocity (V_{in}) (a) $H = 10\ mm$ (b) $H = 30\ mm$

- The lowest value of entropy generation is $\dot{S}_{gen} = 0{,}000479\ W/K$, in this case $H = 30\ mm, F_p = 4.913\ mm, N = 9, H_{rib} = 0.1\ mm, V_{in} = 3\ m/s$. Also, $T_{base} = 24{,}401\ °C$ and $\Delta P = 7{,}512\ Pa$ are obtained. The base plate temperature is 10.64% higher than the lowest possible base plate temperature value. However, there is a significant decrease in ΔP (from 220.88 Pa to 7.512 Pa).

If the design with the least entropy generation is accepted as the optimum design, there will be a slight increase in the base plate temperature while there is a significant decrease in the pressure drop and hence the fan power. As a disadvantage, since the fin height is $H = 30\ mm$, the volume and weight of the heat sink increase.

Symbols

A	Area	cm^2
B	Fin width	mm
CB	Width of channel	mm
CH	Height of channel	mm
d_h	Hydraulic diameter	mm
ΔT	Temperature difference	K
ΔP	Pressure drop	Pa
F_p	Pitch between plate fins	mm
H_{rib}	Rib height	mm
H_{fin}	Fin height	mm
k	Thermal conductivity	W/m-K
L	Fin length	mm
N	Number of fins	-
R_{th}	Thermal resistance	W/K
$\dot{S}_{gen}$	Entropy generation	W/K
t_{hs}	Heat sink base plate thickness	mm
t_{fin}	Fin thickness	mm
T_{in}	Inlet temperature	°C
V_{in}	Inlet velocity	m/s
$\dot{V}_{flow}$	Volumetric flow rate	m^3/s
Pr	Prandtl number	-
$\dot{Q}$	Heat load	W

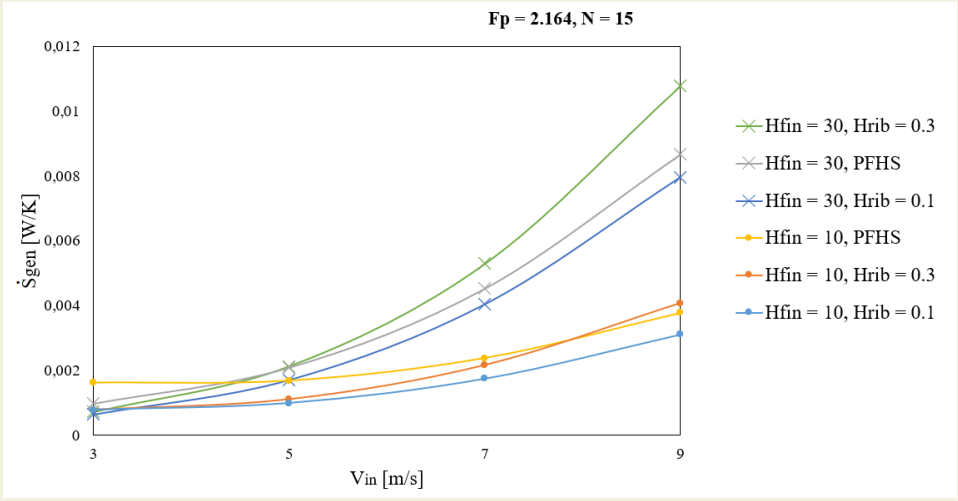

(a)

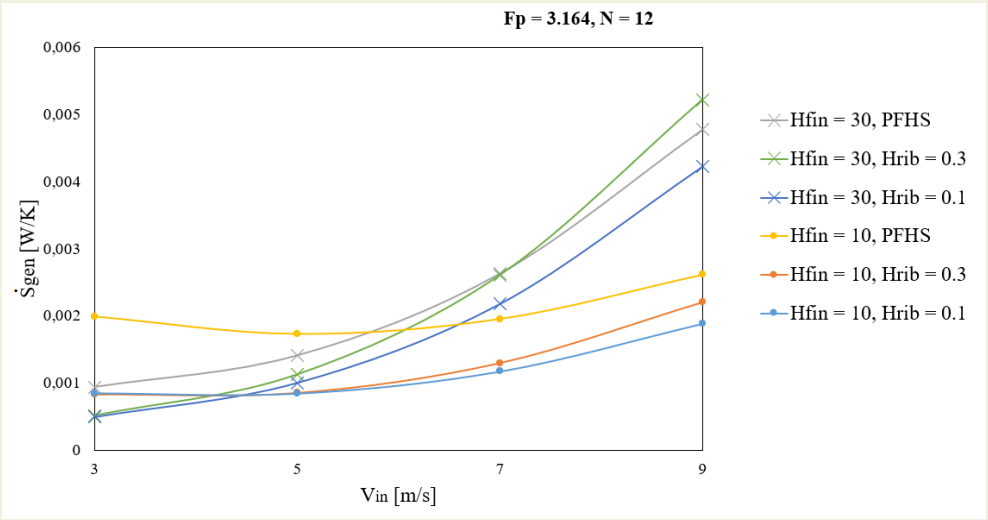

(b)

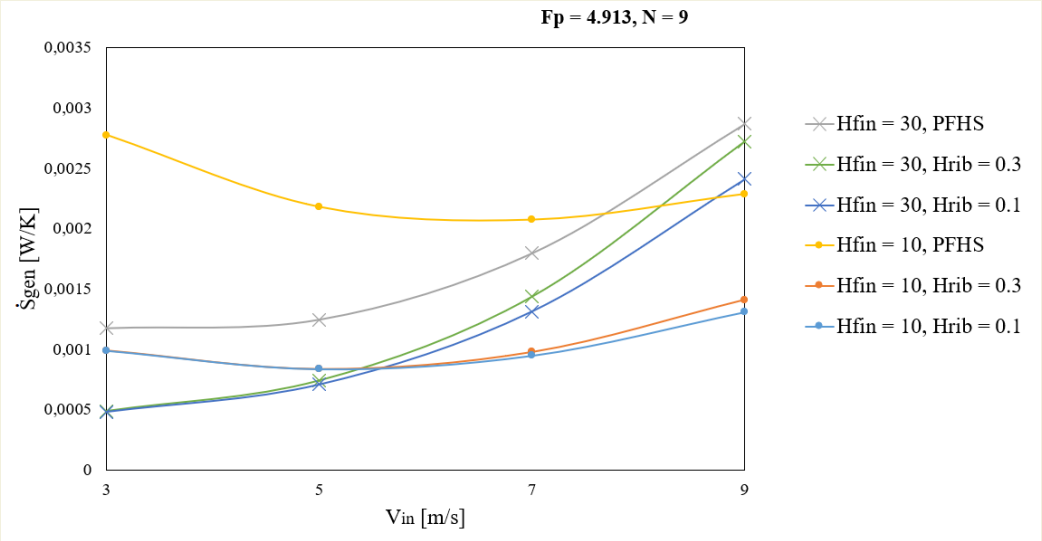

(c)

Figure 10. Entropy generation ($\dot{S}_{gen}$) with inlet velocity (V_{in}) (a) $F_p = 2.164\ mm, N = 15$ (b) $F_p = 3.164\ mm, N = 12$ (c) $F_p = 4.913\ mm, N = 9$

q''	Heat flux	W/m²	ρ_{air}	Density of air	kg/m³
Re_{d_h}	Reynolds number	-	υ	Kinematic viscosity of air	m²/s
y^+	Dimensionless wall distance	-	μ	Dynamic viscosity of air	N-s/m²

References

[1] Bejan, A., (1995). Entropy generation minimization. CRC press Boca Raton, FL.

[2] Kuru, M.N., (2023). Determination of the optimum operating conditions and geometrical dimensions of the plate fin heat sinks using teaching-learning-based-optimization algorithm. Journal of Heat and Mass Transfer. Vol. 145. doi: 10.1115/1.4056299

[3] Yu, X., Feng, J., Feng, Q., Wang, Q., (2005). Development of a plate-pin fin heat sink and its performance comparisons with a plate fin heat sink. Applied Thermal Engineering. 25(2–3): 173–82. doi: 10.1016/j.applthermaleng.2004.06.016.

[4] Yuan, W., Zhao, J., Tso, C.P., Wu, T., Liu, W., Ming, T., (2012). Numerical simulation of the thermal hydraulic performance of a plate pin fin heat sink. Applied Thermal Engineering. 48: 81–8. doi: 10.1016/j.applthermaleng.2012.04.029.

[5] Yamaç, H.İ., Koca, A., (2018). Pin-kanatçık, plaka-kanatçık ve plaka-pin-kanatçıkların soğutma performanslarının sayısal metod kullanılarak karşılaştırılması. Gazi Journal of Engineering Sciences. 4(2): 91–8.

[6] Ayli, E., Bayer, O., Aradag, S., (2016). Experimental investigation and CFD analysis of rectangular profile FINS in a square channel for forced convection regimes. International Journal of Thermal Sciences. 109: 279–90. doi: 10.1016/j.ijthermalsci.2016.06.021.

[7] Inci, A.B., Bayer, Ö., (2019). Experimental and numerical study on heat transfer performance of square, cylindrical and plate heat sinks in external transition flow regime. Journal of Thermal Science and Technology. 39(2): 151–61.

[8] Gupta, A., Kumar, M., Patil, A.K., (2019). Enhanced heat transfer in plate fin heat sink with dimples and protrusions. Heat and Mass Transfer. 55(8): 2247–60. doi: 10.1007/s00231-019-02561-w.

[9] Shaeri, M.R., Yaghoubi, M., (2009). Thermal enhancement from heat sinks by using perforated fins. Energy Conversion and Management. 50(5): 1264–70. doi: 10.1016/j.enconman.2009.01.021.

[10] Ahmed, H.E., Ahmed, M.I., (2015). Optimum thermal design of triangular, trapezoidal and rectangular grooved microchannel heat sinks. International Communications in Heat and Mass Transfer. 66: 47–57. doi: 10.1016/j.icheatmasstransfer.2015.05.009.

[11] Ahmed, H.E., (2016). Optimization of thermal design of ribbed flat-plate fin heat sink. Applied Thermal Engineering. 102: 1422–32. doi: 10.1016/j.applthermaleng.2016.03.119.

[12] Khudhur, D.S., Al-Zuhairy, R.C., and Kassim, M.S., (2022). Thermal analysis of heat transfer with different fin geometry through straight plate-fin heat sinks. International Journal of Thermal Sciences. doi: 10.1016/j.ijthermalsci.2021.107443

[13] Li, H.Y., Chen, C.L., Chao, S.M., Liang, G.F., (2013). Enhancing heat transfer in a plate-fin heat sink using delta winglet vortex generators. International Journal of Heat and Mass Transfer. 67: 666–77. doi: 10.1016/j.ijheatmasstransfer.2013.08.042.

[14] Huang, C.H., Tung, P.W., (2020). Numerical and experimental studies on an optimum Fin design problem to determine the deformed wavy-shaped heat sinks. International Journal of Thermal Sciences. 151(January): 106282. doi: 10.1016/j.ijthermalsci.2020.106282.

[15] Bouchenafa, R., Mohammed, H.A., Saim, R., (2019). Numerical study of the thermal and hydraulic performances of heat sink made of wavy fins. Mechanics and Mechanical Engineering. 23(1): 150–61. doi: 10.2478/mme-2019-0021.

[16] Incropera, F.P., DeWitt, D.P., (1996). Fundamentals of Heat and Mass Transfer. 4th Edition, New York City, New York: John Wiley & Sons, Inc.

[17] Ansys Inc. (2019). Ansys Fluent User's Guide.

[18] White, F.M., (1991). Viscous Fluid Flow, Second Edition. New York: McGraw-Hill.

[19] Mangrulkar, C.K., Dhoble, A.S., Deshmukh, A.R., Mandavgane, S.A., (2017). Numerical investigation of heat transfer and friction factor characteristics from in-line cam shaped tube bank in crossflow. Applied Thermal Engineering. 110: 521–38. doi: 10.1016/j.applthermaleng.2016.08.174.

[20] Jonsson, H., Moshfegh, B., (2001). Modeling of the thermal and hydraulic performance of plate fin, strip fin, and pin fin heat sinks - Influence of flow bypass. IEEE Transactions on Components and Packaging Technologies. 24(2): 142–9. doi: 10.1109/6144.926376.